ISSN: 2350-1278
Peer Reviewed & Refereed Journal (IF: 7.9)
Journal Website: www.nrjitis.in

A THEORETICAL STUDY OF SEMICONDUCTOR BAND STRUCTURE AND CHARGE CARRIER DYNAMICS IN LOW-DIMENSIONAL ELECTRONIC SYSTEMS

Dr. Rajeev Kumar Sharma

Assistant Professor
Dept. of Physics, V. S. J. College, Rajnagar, Madhubani, Lalit Narayan Mithila University, Darbhanga

ABSTRACT

Low-dimensional electronic systems occupy the regime in which at least one device dimension approaches the carrier de Broglie wavelength or mean free path. In this regime, confinement changes the allowed energies, the density of available states and the way in which carriers acquire and lose momentum. This study develops a unified theoretical treatment of these effects and illustrates it with four reproducible calculations. A position-dependent effective-mass Hamiltonian is solved for a $GaAs/Al_{0.3}Ga_{0.7}As$ finite quantum well; dimensional density-of-states functions are compared under common broadening; the transient drift response is evaluated in the relaxation-time approximation; and the thermal evolution of a one-dimensional conductance staircase is obtained from the Landauer formula. For a 0.245 eV conduction-band barrier, reducing the GaAs well width from 20 to 4 nm raises the ground electron subband from 10.10 to 95.39 meV and reduces the number of bound states from five to one. The density of states changes successively from a square-root continuum in three dimensions to steps in two dimensions, threshold singularities in one dimension and discrete peaks in zero dimensions. At an electric field of 1 kV cm^{-1}, relaxation times of 25-100 fs produce steady drift velocities of 6.56-26.25 km s^{-1}, while the corresponding response bandwidth decreases from 6.37 to 1.59 THz. Conductance plateaus remain sharply resolved at 4 K but are progressively rounded when thermal energy approaches the assumed 25 meV subband spacing. The results show that band engineering and carrier dynamics cannot be optimized independently: confinement controls both the spectrum that carriers occupy and the phase space through which they scatter and conduct.

Keywords: quantum confinement; semiconductor nanostructures; quantum wells; density of states; carrier relaxation; ballistic transport; Landauer conductance.

1. INTRODUCTION

The electronic properties of a bulk semiconductor are commonly described by continuous energy bands, three-dimensional crystal momentum and transport coefficients averaged over a large ensemble of scattering events. That description becomes incomplete when a structural dimension is reduced to the nanometre scale. A confining potential then replaces part of the continuous spectrum with discrete subbands, changes the density of final states available for scattering and may make the device length comparable with the mean free path or phase-coherence length. The proposal of compositionally modulated semiconductor superlattices by Esaki and Tsu established that an artificial periodicity could produce minibands and non-classical transport [1]. The subsequent theory of inversion layers, heterojunctions and quasi-two-dimensional gases placed subband formation, screening and magnetotransport within a common framework [2].

Low dimensionality now includes both lithographically or epitaxially confined structures and intrinsically thin crystals. Graphene demonstrated gate-controlled transport in an atomically thin conductor [3], while its low-energy spectrum showed that two-dimensional bands need not remain parabolic but may instead form Dirac cones [4]. Monolayer MoS_2 provided a complementary semiconducting case in which the bulk indirect gap evolves into a direct gap in the one-layer limit [5]. In group-VI dichalcogenides, broken inversion symmetry and spin-orbit coupling additionally lock spin and valley indices near the band edges [6]. These examples make an important theoretical point: dimensionality specifies the kinematic restriction, but orbital character, symmetry, dielectric environment and interactions determine the detailed dispersion.

Confinement is also useful because it alters device response. The step-like density of states of a quantum well can enhance thermoelectric performance under appropriate band and scattering conditions [7]. In quantum dots, size-dependent electron-hole energies underlie the tunability of optical transitions [8]. In a narrow ballistic constriction, transverse quantization gives conductance plateaus in units of $2e^2/h$, as observed in GaAs/AlGaAs point contacts [9]. These phenomena are often discussed separately as band-structure, optical or transport effects, although they originate from the same restricted phase space.

The objective of the present work is to connect these ideas through a compact set of calculations suitable for electronic-science analysis. The study first establishes a hierarchy of band-structure models and then applies a finite effective-mass calculation to a GaAs/AlGaAs quantum well. The resulting subbands are linked to dimensional density-of-states functions. Carrier motion is examined in two limits: a scattering-dominated transient described by a single momentum-relaxation time, and a phase-coherent one-dimensional channel described by Landauer transmission. The selected models do not attempt to reproduce a particular fabricated sample. Their purpose is to isolate the governing scales - well width, barrier height, effective mass, relaxation time, subband spacing and temperature - in a transparent and numerically reproducible form.

2. THEORETICAL FRAMEWORK

From bulk bands to confined subbands

At the most fundamental level, semiconductor bands may be obtained from density-functional theory through the Kohn-Sham equations [10]. For device-scale calculations, however, atomistic tight-binding and continuum envelope-function approaches are frequently more economical. Slater and Koster formulated the transferable two-centre structure used in tight-binding descriptions [11], whereas Kane's multiband treatment showed how coupling between nearby bands modifies effective masses and non-parabolicity [12]. A continuum effective-mass model is most reliable near a non-degenerate band extremum when the confinement varies slowly on the lattice scale; atomistic or multiband methods are required when intervalley coupling, strong non-parabolicity or interface-scale chemistry becomes important [13].

Near a parabolic conduction-band minimum, the inverse effective mass is determined by the band curvature,

$$\frac{1}{m_i^*} = \frac{1}{\hbar^2}\frac{\partial^2 E}{\partial k_i^2}.$$

For a heterostructure grown along z, translational symmetry remains in the $x - y$ plane but is broken in the growth direction. The electron envelope therefore satisfies the position-dependent effective-mass equation

ISSN: 2350-1278
Peer Reviewed & Refereed Journal (IF: 7.9)
Journal Website: www.nrjitis.in

$$\left[-\frac{\hbar^2}{2}\frac{\partial}{\partial z}\left(\frac{1}{m^*(z)}\frac{\partial}{\partial z}\right)+V(z)\right]\psi_n(z)=E_n\psi_n(z).$$

The derivative ordering enforces continuity of the envelope and of $(1/m^*)\partial\psi/\partial z$ across an abrupt interface. In-plane motion remains free, so each confined eigenvalue becomes the edge of a two-dimensional subband,

$$E_n(k_\parallel)=E_n+\frac{\hbar^2\left(k_x^2+k_y^2\right)}{2m_w^*}.$$

The material constants used below are consistent with standard III-V parameter compilations [14]. The single-band approximation also follows the usual device-physics separation between an envelope varying over nanometres and a lattice-periodic Bloch function [15].

DIMENSIONAL DENSITY OF STATES

The density of states (DOS) counts the available quantum states per energy interval. For an isotropic parabolic dispersion in d continuous dimensions, its band-edge dependence is

$$g_d(E)\propto(E-E_c)^{d/2-1}\Theta(E-E_c),$$

where Θ is the Heaviside function. Thus the three-dimensional DOS rises as $\sqrt{E-E_c}$; a two-dimensional subband contributes a constant; a one-dimensional subband produces an inverse-square-root threshold; and a zero-dimensional level contributes a delta function. For a spin-degenerate GaAs two-dimensional electron gas, one occupied parabolic subband has

$$g_{2D}=\frac{m^*}{\pi\hbar^2}=2.80\times10^{13}\ states\ eV^{-1}cm^{-2}$$

for $m^*=0.067m_0$. These distinct functional forms influence screening, optical absorption and scattering because Fermi’s golden rule weights a transition by both its matrix element and its accessible final-state density.

SCATTERING-DOMINATED CARRIER DYNAMICS

Acoustic deformation-potential scattering provides a foundational connection between lattice strain and carrier mobility [16]. Reduced dimensionality can either suppress or enhance scattering: Sakaki predicted that the restricted final-state phase space of an ultrafine wire could strongly suppress selected processes [17], whereas interface roughness and confined phonons may introduce new channels. Detailed high-field transport is normally treated by ensemble Monte Carlo or a full collision integral [18]. For a low-field transient, the relaxation-time Boltzmann equation offers a controlled first approximation [19]:

$$\frac{\partial f}{\partial t}+v\cdot\nabla_r f-\frac{qE}{\hbar}\cdot\nabla_k f=-\frac{f-f_0}{\tau}.$$

For a uniform field switched on at $t=0$, the average drift velocity obeys $dv_d/dt+v_d/\tau=qE/m^*$, giving

$$v_d(t)=\frac{qE\tau}{m^*}\left(1-e^{-t/\tau}\right),\qquad \mu=\frac{q\tau}{m^*}.$$

The same model yields a complex Drude conductivity $\sigma(\omega)=nq^2\tau/[m^*(1-i\omega\tau)]$, with characteristic roll-off frequency $f_c=(2\pi\tau)^{-1}$. Although a single τ does not resolve individual mechanisms, it makes the time-bandwidth trade-off explicit.

BALLISTIC QUANTUM TRANSPORT

When the channel is shorter than the relevant mean free path and phase coherence is retained, resistance is governed by contact injection and quantum transmission. Landauer related conductance to the transmission probability of available modes [20], and Buettiker generalized the approach to phase-coherent multi-terminal conductors [21]. In linear response,

$$G = \frac{2q^2}{h}\int M(E)\,T(E)\left(-\frac{\partial f}{\partial E}\right)dE,$$

where $M(E)$ is the number of propagating modes and $T(E)$ is their transmission. For ideal step transmissions with thresholds E_n,

$$\frac{G}{G_0} = \sum_n \left[1 + exp\left(\frac{E_n - \mu_F}{k_B T}\right)\right]^{-1}, \qquad G_0 = \frac{2q^2}{h}.$$

This expression separates two effects: quantization fixes the height of each fully open mode, while the derivative of the Fermi function rounds its onset over an energy range of order several $k_B T$. Nonequilibrium Green-function methods extend the same open-system viewpoint to self-consistent electrostatics, inelastic scattering and multiband Hamiltonians [22], [23].

3. COMPUTATIONAL METHOD

The numerical study used four linked models. First, the finite quantum-well equation was discretized on a uniform 0.05 nm grid over a 70 nm domain. The interface kinetic coefficient was evaluated from the mean inverse mass at each half-grid point, which is the finite-difference form of the position-dependent operator. Sparse diagonalization returned all eigenvalues below the 0.245 eV barrier. Well widths from 4 to 20 nm were examined. The continuum edges of the barrier were not counted as bound states.

Second, parabolic DOS functions were evaluated from 0 to 120 meV. To make the dimensional singularities visible on a finite grid, the ideal spectra were convolved with a Gaussian of standard deviation 2 meV. Each dimensional curve was normalized to its own maximum; consequently, Figure 2 compares spectral shape rather than absolute units. The two-, one- and zero-dimensional cases used thresholds at 0, 30, 60 and 90 meV. Third, the transient drift equation was evaluated for a GaAs electron under a step field of 1 kV cm^{-1}, using $\tau = 25$, 50 and 100 fs. These values span a useful range from strongly damped to comparatively persistent momentum response while remaining within the low-field parabolic-band model. Fourth, ideal one-dimensional conductance was calculated for five spin-degenerate modes separated by 25 meV at 4, 77 and 300 K. Numerical integration of the general Landauer expression and the closed-form Fermi-weighted sum agreed to machine precision. The ballistic formulation follows the standard mesoscopic transport treatment [24].

Table I. Parameters used in the theoretical calculations

Parameter	Symbol	Value	Role or basis
GaAs electron effective mass	m_w^*	$0.067m_0$	Well dispersion [14]
$Al_{0.3}Ga_{0.7}As$ electron mass	m_b^*	$0.0919m_0$	Linear alloy interpolation [14]
Conduction-band barrier	V_0	0.245 eV	Finite-well benchmark [14]
Spatial grid	Δz	0.05 nm	Eigenvalue discretization

DOS broadening	γ	2 meV	Common Gaussian resolution
Applied field	E	1 kV cm^{-1}	Low-field transient
Relaxation times	τ	25, 50, 100 fs	Drude-Boltzmann comparison
1D subband spacing	ΔE	25 meV	Ideal quantum point contact
Temperatures	T	4, 77, 300 K	Thermal broadening comparison

4. RESULTS AND DISCUSSION

Confinement-driven band reconstruction

Figure 1(a) shows the finite barrier and the three bound electron states of a 10 nm well. The ground state lies at 30.39 meV and is concentrated near the centre; the second state at 119.33 meV has one node; the third state at 240.83 meV is only weakly bound and therefore penetrates substantially into the AlGaAs barrier. This leakage is physically important because an infinite-well model would force every wavefunction to zero at the interface and would overestimate the energy of the more weakly confined states. Figure 1(b) converts these discrete values into parabolic in-plane subbands. The energy remains quantized along z but continuous in $k_{\parallel}$, which is precisely the spectrum of a quasi-two-dimensional electron gas.

The width dependence in Figure 1(c) reveals both a continuous energy shift and a discrete change in the number of bound modes. At 4 nm, only one state remains below the barrier and its energy is 95.39 meV. A second, weakly bound level appears at 5 nm. Three bound states are supported at 10-12 nm, four at 15 nm and five at 20 nm. Across the full range, the ground-state energy falls by 89.4%, from 95.39 to 10.10 meV. The trend approaches the L^{-2} scaling of an infinite square well for stronger confinement, but finite-barrier penetration softens that dependence. The calculation demonstrates why geometric tolerances of only a few monolayers can produce measurable shifts in intersubband and optical-transition energies.

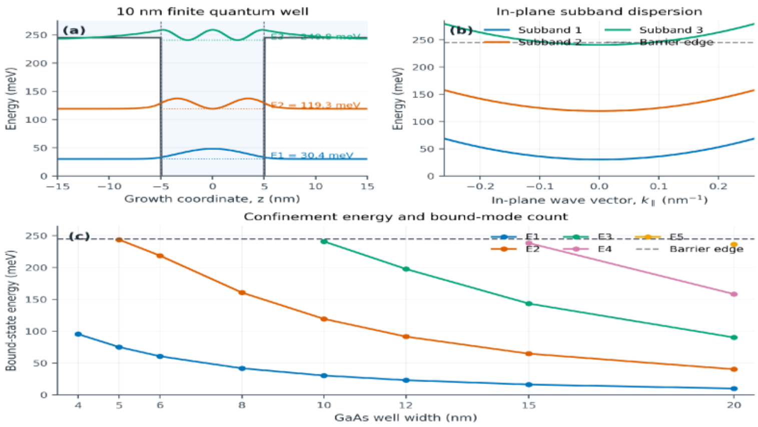

Figure 1. Finite-well band structure. (a) GaAs/AlGaAs potential and scaled probability-density profiles at a 10 nm width; traces are vertically offset to their eigenenergies. (b) In-plane parabolic dispersion of the three bound subbands. (c) Bound-state energies as a function of well width; the dashed line is the barrier edge.

Table II. Calculated conduction-subband energies for the finite GaAs well

Well width (nm)	E_1 (meV)	E_2 (meV)	E_3 (meV)	Bound states below 0.245 eV
4	95.39	-	-	1

5	75.19	243.69	-	2
6	60.63	218.52	-	2
8	41.71	160.54	-	2
10	30.39	119.33	240.83	3
12	23.11	91.49	197.65	3
15	16.26	64.71	143.32	4
20	10.10	40.31	90.21	5

Density-of-states signatures

Figure 2 makes visible the spectral reorganization that accompanies each reduction in dimensionality. The three-dimensional curve increases smoothly because the number of constant-energy k states grows with the surface area of a sphere. Confinement in one direction divides the spectrum into two-dimensional subbands, each adding a constant DOS and producing a staircase. Confinement in two directions leaves a one-dimensional propagation axis; the small group velocity near each subband minimum then creates a strong van Hove threshold. Full confinement produces discrete zero-dimensional lines. The imposed 2 meV Gaussian broadening turns ideal discontinuities and delta functions into finite features analogous to finite lifetime or instrumental resolution.

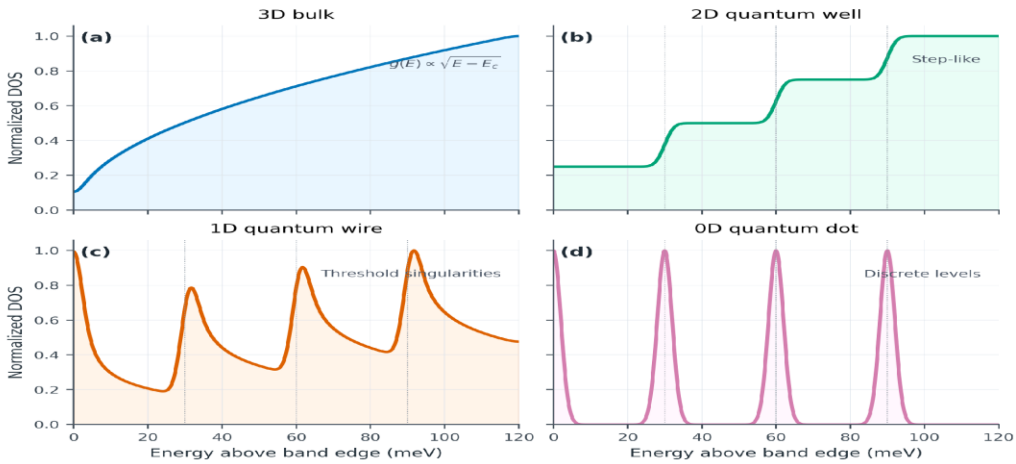

Figure 2. Dimensional evolution of the parabolic-band density of states. Each spectrum is normalized independently. A common 2 meV Gaussian broadening is applied; thresholds for the confined cases are 0, 30, 60 and 90 meV.

This hierarchy clarifies why the same perturbation can have different transport consequences in different devices. When the Fermi level crosses a 2D subband edge, the scattering phase space changes abruptly but remains finite. Near a 1D threshold, the large DOS can enhance processes whose matrix elements connect the relevant states, even though other backscattering channels may be restricted. In a quantum dot, transport becomes resonance-selective because there is no continuum of final orbital states within the dot. Consequently, the statement that dimensional reduction simply increases mobility is not general; the result depends on which disorder, phonon or Coulomb process is dominant and on where the chemical potential lies relative to a DOS feature.

RELAXATION TIME, DRIFT RESPONSE AND BANDWIDTH

The calculated velocity transients in Figure 3 rise monotonically after the field is applied. A shorter relaxation time establishes steady state rapidly but yields a smaller terminal velocity because momentum is lost more frequently. With $\tau = 25$ fs, the drift velocity reaches 98% of its 6.56 km s^{-1} asymptote in approximately 0.10 ps. For $\tau = 100$ fs, the velocity is still evolving at 0.3 ps and approaches 26.25 km s^{-1} only after several hundred femtoseconds. The corresponding low-field mobilities are 656, 1313 and 2625 $cm^2\ V^{-1}\ s^{-1}$.

There is a complementary frequency-domain interpretation. Increasing τ raises dc mobility but lowers the Drude roll-off frequency from 6.37 THz at 25 fs to 1.59 THz at 100 fs. This does not mean that a high-mobility material is intrinsically slow; it means that the momentum distribution retains memory for longer and the simple intraband conductivity cannot follow arbitrarily rapid field reversals. In a real low-dimensional device, optical-phonon emission, intervalley transfer, carrier heating and non-parabolicity make τ energy dependent. The present curves nevertheless separate the basic inertia-relaxation balance from those additional effects.

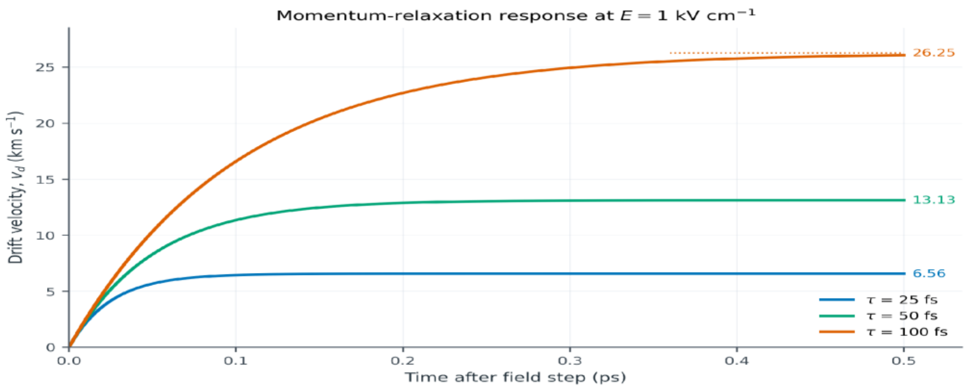

Figure 3. Transient electron drift velocity in GaAs after application of a 1 kV cm^{-1} step field. Dashed horizontal segments mark the calculated steady-state velocities.

Table III. Drude response obtained from the three relaxation times

τ (fs)	Mobility ($cm^2\ V^{-1}\ s^{-1}$)	v_∞ (km s^{-1})	f_c (THz)
25	656	6.56	6.37
50	1313	13.13	3.18
100	2625	26.25	1.59

Thermal broadening of quantized conductance

At 4 K, k_BT is only 0.345 meV, far below the 25 meV mode spacing. Figure 4 therefore shows flat plateaus separated by sharp rises, and each fully transmitted spin-degenerate mode contributes one $G_0 = 2e^2/h$. At 77 K, $k_BT = 6.64$ meV and the transitions overlap modestly, although the first four plateaus remain identifiable. At 300 K, $k_BT = 25.85$ meV, essentially equal to the assumed separation. The staircase is then transformed into a smooth increase: at a chemical potential 85 meV above the first threshold, the conductance is 4.000 G_0 at 4 K, 3.908 G_0 at 77 K and 3.624 G_0 at 300 K.

The rounding is not caused by additional scattering in this calculation. Transmission remains unity for every open mode; temperature alone broadens the injection window. This distinction matters when interpreting measured plateaus. Imperfect transmission lowers or distorts a plateau, whereas thermal broadening smooths its edges through reservoir occupation. Contact resistance is also not an extraneous correction in the Landauer picture: it is the finite resistance associated with injecting a limited number of modes. The same viewpoint explains why reducing a channel length does not drive a two-terminal ballistic resistance to zero.

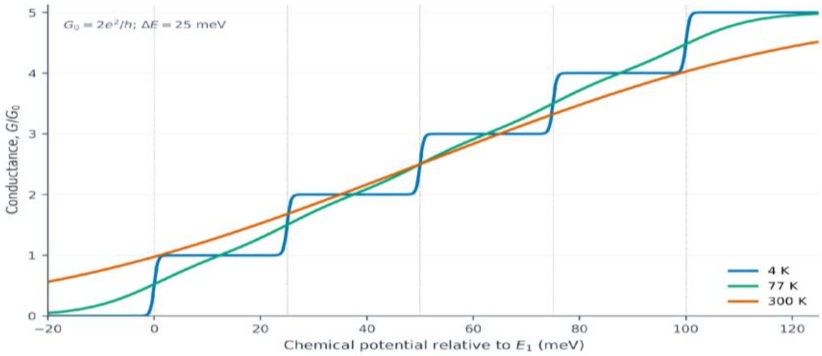

Figure 4. Ideal spin-degenerate Landauer conductance for five one-dimensional modes separated by 25 meV. Thermal occupation rounds the quantized staircase as k_BT approaches the mode spacing.

5. IMPLICATIONS AND MODEL BOUNDARIES

The combined results identify three design rules. First, confinement energy and mode count are set jointly by width and barrier height; a nominal well width cannot be interpreted without the surrounding band offsets and mass mismatch. Second, DOS engineering alters both useful response and unwanted scattering. A large near-edge DOS may improve absorption or thermopower, yet it can also increase a transition rate if the perturbing matrix element remains strong. Third, the appropriate transport formalism depends on length and time scales. A relaxation-time model is informative when many randomizing events occur, while a transmission model is natural when a small number of coherent modes connects reservoirs.

The numerical values should be read within the assumptions of the models. The quantum-well calculation neglects strain, self-consistent Hartree fields, exchange-correlation effects and conduction-band non-parabolicity. The DOS comparison uses a common phenomenological broadening rather than a calculated self-energy. The drift calculation assumes a constant τ, and the Landauer channel assumes perfect adiabatic contacts and no inelastic scattering. Strongly confined III-V structures may require a multiband $k \cdot p$ Hamiltonian, while graphene and other atomically thin lattices require symmetry-appropriate tight-binding or first-principles bands rather than a scalar GaAs mass. For biased nanodevices, self-consistent nonequilibrium Green functions provide the systematic route from the present idealized limits to electrostatic charging and energy-dependent scattering [22], [23].

CONCLUSION

A single theoretical framework can connect semiconductor band reconstruction with carrier dynamics across quantum wells, wires and dots. The finite GaAs/AlGaAs calculation showed that reducing the well width from 20 to 4 nm raises the ground subband nearly tenfold and removes four bound modes. The DOS analysis demonstrated that this spectral quantization changes the energy dependence of available states from a smooth three-dimensional continuum to steps, singular thresholds and discrete resonances. The transient calculation linked momentum-relaxation time to both mobility and terahertz response, while the

Landauer calculation showed that conductance quantization survives only when thermal broadening is small relative to subband spacing.

The central result is therefore not merely that smaller structures possess larger level separations. Confinement reorganizes the spectrum, occupation, scattering phase space and contact injection simultaneously. Device design should consequently treat well width, carrier mass, barrier composition, temperature and relaxation mechanisms as a coupled set of variables. More elaborate multiband or atomistic calculations can refine the numerical values, but the effective-mass, Boltzmann and Landauer limits remain valuable because they expose the physical scales that govern low-dimensional electronic systems.

REFERENCES

1. L. Esaki and R. Tsu, "Superlattice and negative differential conductivity in semiconductors," IBM Journal of Research and Development, vol. 14, no. 1, pp. 61–65, 1970.

2. T. Ando, A. B. Fowler, and F. Stern, "Electronic properties of two-dimensional systems," Reviews of Modern Physics, vol. 54, no. 2, pp. 437–672, 1982.

3. K. S. Novoselov et al., "Electric field effect in atomically thin carbon films," Science, vol. 306, no. 5696, pp. 666–669, 2004.

A. H. Castro Neto, F. Guinea, N. M. R. Peres, K. S. Novoselov, and A. K. Geim, "The electronic properties of graphene," Reviews of Modern Physics, vol. 81, no. 1, pp. 109–162, 2009.

4. K. F. Mak, C. Lee, J. Hone, J. Shan, and T. F. Heinz, "Atomically thin MoS_2: A new direct-gap semiconductor," Physical Review Letters, vol. 105, no. 13, Art. no. 136805, 2010.

5. D. Xiao, G.-B. Liu, W. Feng, X. Xu, and W. Yao, "Coupled spin and valley physics in monolayers of MoS_2 and other group-VI dichalcogenides," Physical Review Letters, vol. 108, no. 19, Art. no. 196802, 2012.

6. L. D. Hicks and M. S. Dresselhaus, "Effect of quantum-well structures on the thermoelectric figure of merit," Physical Review B, vol. 47, no. 19, pp. 12727–12731, 1993.

7. L. E. Brus, "Electron-electron and electron-hole interactions in small semiconductor crystallites: The size dependence of the lowest excited electronic state," The Journal of Chemical Physics, vol. 80, no. 9, pp. 4403–4409, 1984.

8. B. J. van Wees et al., "Quantized conductance of point contacts in a two-dimensional electron gas," Physical Review Letters, vol. 60, no. 9, pp. 848–850, 1988.

9. W. Kohn and L. J. Sham, "Self-consistent equations including exchange and correlation effects," Physical Review, vol. 140, no. 4A, pp. A1133–A1138, 1965.

10. J. C. Slater and G. F. Koster, "Simplified LCAO method for the periodic potential problem," Physical Review, vol. 94, no. 6, pp. 1498–1524, 1954.

11. E. O. Kane, "Band structure of indium antimonide," Journal of Physics and Chemistry of Solids, vol. 1, no. 4, pp. 249–261, 1957.

12. P. Harrison and A. Valavanis, Quantum Wells, Wires and Dots: Theoretical and Computational Physics of Semiconductor Nanostructures, 4th ed. Chichester, U.K.: Wiley, 2016.

13. Vurgaftman, J. R. Meyer, and L. R. Ram-Mohan, "Band parameters for III–V compound semiconductors and their alloys," Journal of Applied Physics, vol. 89, no. 11, pp. 5815–5875, 2001.

14. S. M. Sze and K. K. Ng, Physics of Semiconductor Devices, 3rd ed. Hoboken, NJ, USA: Wiley, 2006.

15. Bardeen and W. Shockley, "Deformation potentials and mobilities in non-polar crystals," Physical Review, vol. 80, no. 1, pp. 72–80, 1950.

16. H. Sakaki, "Scattering suppression and high-mobility effect of size-quantized electrons in ultrafine semiconductor wire structures," Japanese Journal of Applied Physics, vol. 19, no. 12, pp. L735–L738, 1980.

17. C. Jacoboni and L. Reggiani, "The Monte Carlo method for the solution of charge transport in semiconductors with applications to covalent materials," Reviews of Modern Physics, vol. 55, no. 3, pp. 645–705, 1983.

18. M. Lundstrom, Fundamentals of Carrier Transport, 2nd ed. Cambridge, U.K.: Cambridge University Press, 2000.

19. R. Landauer, "Spatial variation of currents and fields due to localized scatterers in metallic conduction," IBM Journal of Research and Development, vol. 1, no. 3, pp. 223–231, 1957.

20. M. Buettiker, "Four-terminal phase-coherent conductance," Physical Review Letters, vol. 57, no. 14, pp. 1761–1764, 1986.

21. S. Datta, Electronic Transport in Mesoscopic Systems. Cambridge, U.K.: Cambridge University Press, 1995.

22. R. Lake, G. Klimeck, R. C. Bowen, and D. Jovanovic, "Single and multiband modeling of quantum electron transport through layered semiconductor devices," Journal of Applied Physics, vol. 81, no. 12, pp. 7845–7869, 1997.

23. C. W. J. Beenakker and H. van Houten, "Quantum transport in semiconductor nanostructures," Solid State Physics, vol. 44, pp. 1–228, 1991.